AIP | Journal of Applied Physics

Analytical model for current distribution in large-area organic light emitting diodes with parallel metal grid lines

Marco Barink and Stephan Harkema

Citation: J. Appl. Phys. **112**, 054507 (2012); doi: 10.1063/1.4749419
View online: http://dx.doi.org/10.1063/1.4749419
View Table of Contents: http://jap.aip.org/resource/1/JAPIAU/v112/i5
Published by the American Institute of Physics.

Analytical model for current distribution in large-area organic light emitting diodes with parallel metal grid lines

Marco Barink[1,a)] and Stephan Harkema[2]
[1]*Netherlands Organization for Applied Scientific Research (TNO), P.O. Box 6235, 5600 HE, Eindhoven, The Netherlands*
[2]*Holst Centre/TNO, P.O. Box 8550, 5605 KN, Eindhoven, The Netherlands*

(Received 4 April 2012; accepted 9 August 2012; published online 7 September 2012)

In this study, an analytical solution for the current distribution of a large-area organic light emitting diodes (OLEDs) with parallel equidistant gridlines is derived. In contrast to numerical methods, this analytical solution allows for a very quick scan of the OLED design space, even for very large OLEDs, providing insight how different model parameters affect each other. The assumptions within the analytical derivation are verified with finite element simulations of the same OLED. Furthermore, the analytically calculated light distribution was experimentally verified by measuring the light distribution on a large-area OLED. © *2012 American Institute of Physics*. [http://dx.doi.org/10.1063/1.4749419]

I. INTRODUCTION

Flexible organic light emitting diodes (OLEDs) are very thin and light-weight light sources which are expected to revolutionarize the way we apply and experience light within office, home and urban environment.[1–5] The current light bulbs will be replaced with intelligent large area lighting: lighting which allows for all kinds of customization by the user, like cutting and bending. The future will probably provide some sort of electronic wallpaper which can be adapted by remote control.

An OLED can be regarded as a thin layer of light emitting material (organic semiconductor) which is sandwiched between an anode and a cathode. As the light has to be able to escape from the OLED, one of these two, anode or cathode, needs to be transparent. Therefore, transparent conductors are applied, like indium-tin-oxide (ITO) or poly(3,4-ethylenedioxythiophene) poly(styrenesulfonate) (PEDOT:PSS). However, these transparent conductors are still fairly bad electrical conductors in comparison to metals. For large-area OLEDs, this leads to an inhomogeneous potential and current distribution over the OLED and thereby to an inhomogeneous light output. This inhomogeneity increases with increasing OLED area.

Currently, flexible OLEDs are still relatively small, in the order of a few square centimeters. The near future will show a race towards larger and larger OLEDs with a good light homogeneity and a low power input. These demands are contradictory as long as the resistance of the transparent anode or cathode remains unchanged.

However, the application of thin metal grids to enhance the conductivity of the transparent OLED electrode brings large area OLEDs within reach.[1,6–9] Such grids allow for larger OLED tiles while still maintaining a reasonable power consumption and light homogeneity. A schematic overview of an OLED with a metal grid is shown in Figure 1. In this device configuration, the anode of the OLED is formed by a combination of metal gridlines and the transparent conductive polymer PEDOT:PSS. In order to achieve an efficient injection of current into the OLED, two bus bars consisting of aluminum are placed on both sides of the grid. The thickness of the different layers is in the order of 100–500 nm. The planar dimensions of the OLED can be in the order of centimeters.

Modeling tools are used to optimize the grid pattern dimensions and to predict the light homogeneity of OLEDs.[7] Typically, finite element (FEM) and finite difference methods[8,10] are very suitable to solve this kind of conductivity distribution problems. However, due to the extreme aspect ratio of the OLED tile (μm thickness vs. cm in planar directions) and differences in dimensions of the OLED structures (nm layer thickness, vs. μm grid dimensions, vs. cm OLED dimensions), large OLED tiles are very difficult to model numerically, as an extremely large amount of elements is required.

It is therefore preferable to use analytical models, since they do not have this disadvantage. Furthermore, numerical simulations may sometimes seem like a black box, analytical equations may help to provide insight in how the different parameters affect the result. However, very complex geometries are impossible to model analytically.

Choi *et al.*[6] presented an analytical model of an OLED with equidistant lines. However, they ignored the voltage drop along the metal grid, simplifying the voltage drop to a 1-dimensional issue. This was a reasonable assumption as their OLED area was relatively small (7.3 cm^2) and furthermore they used relatively thick metal lines with a high conductivity (electroplated copper which was patterned using lithography). However, in practice, thick metal lines mean more topology (a very thin light emitting layer has to be deposited over the grid lines), more material and therefore higher costs. Furthermore, for large-area OLEDs, preferably printed metal lines are used that exhibit a 5–7 times lower conductivity as compared to the bulk values of the metal.

a)Author to whom correspondence should be addressed. Electronic mail: marco.barink@tno.nl. Tel.: +31 888665664. Fax: +31 888668847.

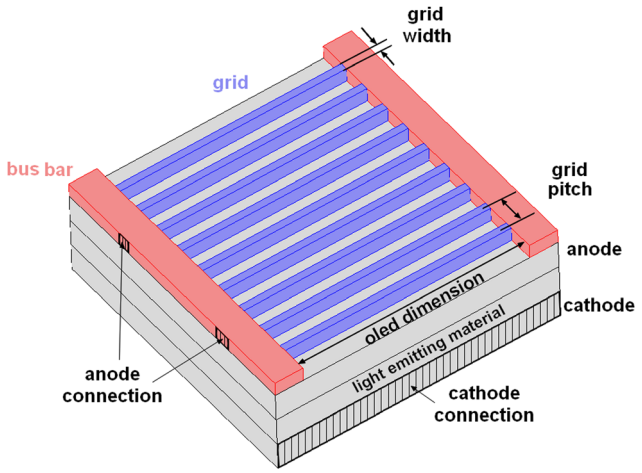

FIG. 1. Schematic drawing of an OLED with bus bars (red) and gridlines (blue).

When using these practically more realistic specifications on OLED area and grid properties, the voltage drop along the metal grid needs to be taken into account.

The aim of this study was to determine and validate a more sophisticated analytical solution of the light output for large OLEDs (up to dimensions of tens of cm) with a thin metal grid consisting of parallel equidistant lines. For validation, the analytical solution was compared with FEM calculations of the same problem to verify the validity of several assumptions. Furthermore, the calculated analytical light distribution was also verified by experiments on large-area OLEDs. As a final result, an example of a design space for the light distribution in an OLED is given, to illustrate the applicability of this analytical approach. When a given homogeneity of a large-area OLED is required the analytical solution provides a fast and direct way to predict the optimal grid design.

II. DERIVATION OF AN ANALYTICAL SOLUTION

Figure 2 shows a very small part of the OLED in Figure 1: only an area containing half the width of a gridline (b1), half the distance between two gridlines (l), and half the distance between both bus bars (l2). The bus bar would be at the left side of the figure, but is omitted together with the cathode. Figure 3 is the cross section as shown in Figure 2. The light emitting layer is labeled as light emitting polymer (LEP). However, this can be any kind of emitter stack.

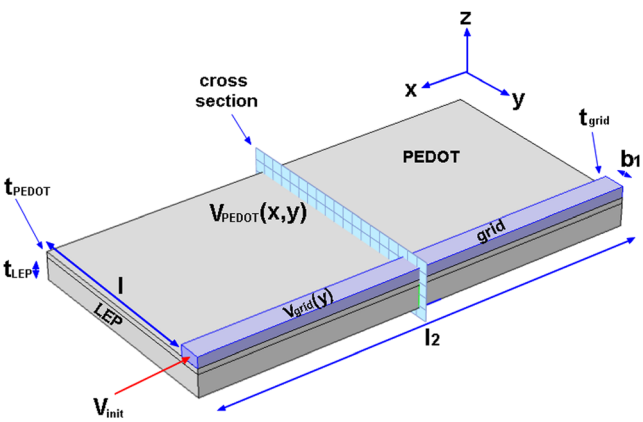

FIG. 2. Overview of a unit cell of the OLED. Note that the bus bar and cathode are omitted.

The derivation is started with the steady state continuity equation for currents (div(j) = 0) within the PEDOT anode (Figures 2 and 3), where j_1, j_2, and j_3 are the currents in the x, y, and z direction and t_{pedot}, t_{grid}, and t_{lep} are the thicknesses of the PEDOT, grid, and LEP layers, respectively. It is assumed that there is no x-component for the current within the PEDOT, as in general the length of the gridlines will be much longer than the distance between them. Hence,

$$\frac{\partial j_2}{\partial y} + \frac{\partial j_3}{\partial z} = 0, \tag{1}$$

$$\frac{\partial j_3}{\partial z} = \frac{j_{lep}}{t_{pedot}}, \tag{2}$$

which leads to

$$\frac{\partial j_2}{\partial y} + \frac{j_{lep}}{t_{pedot}} = 0. \tag{3}$$

Ohm's law then relates the current density to the electric potential V_i

$$j_i = \sigma \cdot E = -\sigma \cdot \nabla V_i, \tag{4}$$

$$-\sigma_{pedot} \cdot \frac{\partial^2 V_{pedot}}{\partial y^2} + \frac{j_{lep}}{t_{pedot}} = 0, \tag{5}$$

$$j_{lep} = \frac{V_{pedot}(y) - V_{th}}{r}. \tag{6}$$

With σ_{pedot}, the conductivity of the PEDOT:PSS and V_{pedot} the electric potential within the PEDOT:PSS. The V_{th} is a threshold value for the linearization of the current density—voltage (j-V) curve of the OLED and r the slope of the linearization (Figure 4). Note that this is only correct when it is assumed that the whole cathode is grounded (V = 0). The j-V curve was measured on a small area intrinsic OLED without grid

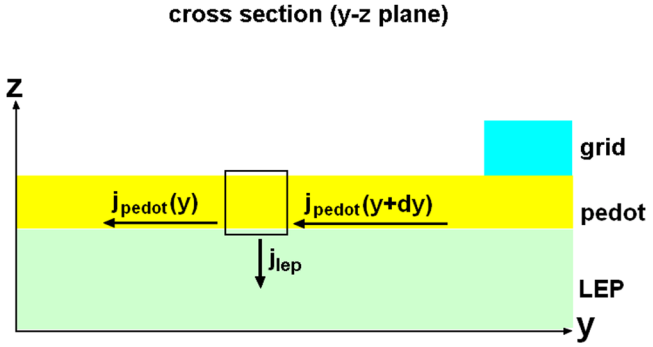

FIG. 3. Schematic current flow within PEDOT: PSS.

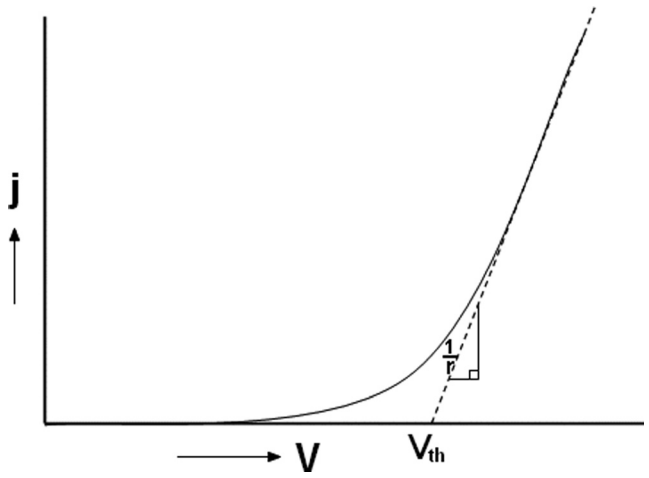

FIG. 4. Schematic j-V-curve of a small area intrinsic OLED without grid.

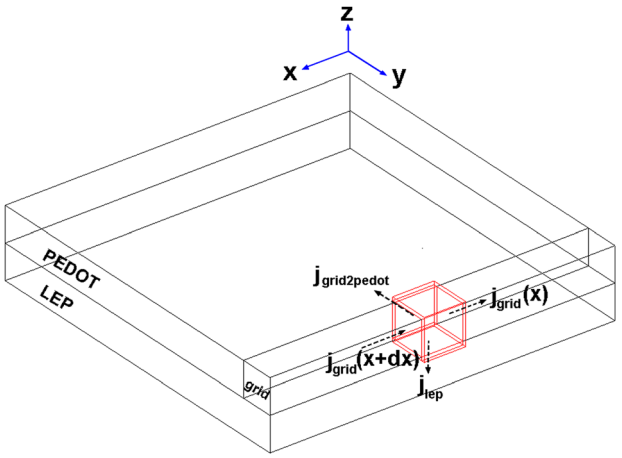

FIG. 5. Schematic current flow within the gridline.

$$\frac{\partial^2 V_{pedot}}{\partial y^2} - \frac{V_{pedot}(y) - V_{th}}{r \cdot \sigma_{pedot} \cdot t_{pedot}} = 0, \tag{7}$$

which has the following general solution

$$V_{pedot}(y) = A_1 e^{\frac{1}{\Lambda} y} + A_2 e^{-\frac{1}{\Lambda} y} + A_3, \tag{8}$$

with

$$\frac{1}{\Lambda^2} = \frac{1}{r \cdot \sigma_{pedot} \cdot t_{pedot}}. \tag{9}$$

This equation can be solved using an assumption of symmetry (Eq. (10)), and with the assumption that the voltage within the gridline is known (Eq. (11))

$$\frac{\partial V_{pedot}(0)}{\partial y} = 0, \tag{10}$$

$$V_{pedot}(l) = V_{grid}(x), \tag{11}$$

V_{grid} is the electric potential within the grid. Combining the general solution with the assumptions results in the following solution for the voltage within the PEDOT:

$$V_{pedot}(x,y) = \left(\frac{V_{grid}(x) - V_{th}}{e^{\frac{1}{\Lambda} l} + e^{-\frac{1}{\Lambda} l}}\right) \cdot e^{\frac{1}{\Lambda} y} + \left(\frac{V_{grid}(x) - V_{th}}{e^{\frac{1}{\Lambda} l} + e^{-\frac{1}{\Lambda} l}}\right) \cdot e^{-\frac{1}{\Lambda} y} + V_{th}. \tag{12}$$

Within this solution, $V_{grid}(x)$ is still unknown. $V_{grid}(x)$ can be determined in a similar way with the continuity equation for currents, but now for the gridline. Figure 5 shows a similar image as Figure 2, with the difference that Figure 5 shows a small box with a schematic current overview. For simplicity, it is assumed that the PEDOT is only next to the gridline, and that the LEP is below the PEDOT and the gridline

$$\frac{\partial j_1}{\partial x} + \frac{\partial j_2}{\partial y} + \frac{\partial j_3}{\partial z} = 0, \tag{13}$$

$$\frac{\partial j_2}{\partial y} = \frac{j_{grid2pedot}}{b_1}, \tag{14}$$

$$\frac{\partial j_3}{\partial z} = \frac{j_{lep}}{t_{grid}} = \frac{V_{grid}(x) - V_{th}}{r \cdot t_{grid}}. \tag{15}$$

With $j_{grid2pedot}$, the current flow from the grid to the PEDOT. So,

$$\frac{\partial j_1}{\partial x} + \frac{j_{grid2pedot}}{b_1} + \frac{V_{grid}(x) - V_{th}}{r \cdot t_{grid}} = 0, \tag{16}$$

$$j_i = \sigma \cdot E = -\sigma \cdot \nabla V_i, \tag{17}$$

$$-\sigma_{grid} \cdot \frac{\partial^2 V_{grid}}{\partial x^2} + \frac{j_{grid2pedot}}{b_1} + \frac{V_{grid}(x) - V_{th}}{r \cdot t_{grid}} = 0, \tag{18}$$

$$\begin{aligned} j_{grid2pedot} &= j_{pedot}(x,l) \cdot \frac{t_{pedot}}{t_{grid}} = \sigma_{pedot} \cdot \frac{\partial V_{pedot}(x,l)}{\partial y} \cdot \frac{t_{pedot}}{t_{grid}} \\ &= \sigma_{pedot} \cdot \frac{t_{pedot}}{t_{grid}} \cdot \left[\left(\frac{V_{grid}(x) - V_{th}}{e^{\frac{1}{\Lambda} l} + e^{-\frac{1}{\Lambda} l}}\right) \cdot \frac{1}{\Lambda} \cdot e^{\frac{1}{\Lambda} l} - \left(\frac{V_{grid}(x) - V_{th}}{e^{\frac{1}{\Lambda} l} + e^{-\frac{1}{\Lambda} l}}\right) \cdot \frac{1}{\Lambda} \cdot e^{-\frac{1}{\Lambda} l}\right] \\ &= \left[\frac{\sigma_{pedot}}{\Lambda} \cdot \frac{t_{pedot}}{t_{grid}} \cdot \left(\frac{e^{\frac{1}{\Lambda} l} - e^{-\frac{1}{\Lambda} l}}{e^{\frac{1}{\Lambda} l} + e^{-\frac{1}{\Lambda} l}}\right)\right] \cdot \left(V_{grid}(x) - V_{th}\right). \end{aligned} \tag{19}$$

Filling this in within the former equation (and performing a little rework) gives

$$\frac{\partial^2 V_{grid}}{\partial x^2} - \left[\frac{\sigma_{pedot}}{\sigma_{grid}\cdot\Lambda\cdot b_1}\cdot\frac{t_{pedot}}{t_{grid}}\cdot\left(\frac{e^{\frac{1}{\Lambda}\cdot l}-e^{-\frac{1}{\Lambda}\cdot l}}{e^{\frac{1}{\Lambda}\cdot l}+e^{-\frac{1}{\Lambda}\cdot l}}\right)\right]\cdot\left(V_{grid}(x)-V_{th}\right) - \frac{V_{grid}(x)-V_{th}}{\sigma_{grid}\cdot r\cdot t_{grid}}$$
$$= \frac{\partial^2 V_{grid}}{\partial x^2} - \left[\frac{\sigma_{pedot}}{\sigma_{grid}\cdot\Lambda\cdot b_1}\cdot\frac{t_{pedot}}{t_{grid}}\cdot\left(\frac{e^{\frac{1}{\Lambda}\cdot l}-e^{-\frac{1}{\Lambda}\cdot l}}{e^{\frac{1}{\Lambda}\cdot l}+e^{-\frac{1}{\Lambda}\cdot l}}\right)+\frac{1}{\sigma_{grid}\cdot r\cdot t_{grid}}\right]\cdot V_{grid}(x)$$
$$+\left[\frac{\sigma_{pedot}}{\sigma_{grid}\cdot\Lambda\cdot b_1}\cdot\frac{t_{pedot}}{t_{grid}}\cdot\left(\frac{e^{\frac{1}{\Lambda}\cdot l}-e^{-\frac{1}{\Lambda}\cdot l}}{e^{\frac{1}{\Lambda}\cdot l}+e^{-\frac{1}{\Lambda}\cdot l}}\right)+\frac{1}{\sigma_{grid}\cdot r\cdot t_{grid}}\right]\cdot V_{th}. \quad (20)$$

This can again be solved with

$$\frac{\partial V_{grid}(0)}{\partial y} = 0, \quad (21)$$

$$V_{grid}(l_2) = V_{init}, \quad (22)$$

which are similar assumptions as used in Eqs. (10) and (11). This gives, analogous to Eqs. (8)–(12)

$$\frac{1}{\Lambda_2} = \sqrt{\frac{\sigma_{pedot}}{\sigma_{grid}\cdot\Lambda\cdot b_1}\cdot\frac{t_{pedot}}{t_{grid}}\cdot\left(\frac{e^{\frac{1}{\Lambda}\cdot l}-e^{-\frac{1}{\Lambda}\cdot l}}{e^{\frac{1}{\Lambda}\cdot l}+e^{-\frac{1}{\Lambda}\cdot l}}\right)+\frac{1}{\sigma_{grid}\cdot r\cdot t_{grid}}}, \quad (23)$$

$$V_{grid}(x) = \left(\frac{V_{init}-V_{th}}{e^{\frac{1}{\Lambda_2}\cdot l_2}+e^{-\frac{1}{\Lambda_2}\cdot l_2}}\right)\cdot e^{\frac{1}{\Lambda_2}\cdot x} + \left(\frac{V_{init}-V_{th}}{e^{\frac{1}{\Lambda_2}\cdot l_2}+e^{-\frac{1}{\Lambda_2}\cdot l_2}}\right)\cdot e^{-\frac{1}{\Lambda_2}\cdot x} + V_{th}. \quad (24)$$

The relation between the luminance (cd/m^2) and the electric potential V is similar to the relation between the current density j and the electric potential V. Hence, the luminance L can easily be determined from the electric potential by

$$L = b\cdot\left(V(x,y)-V_{th}\right). \quad (25)$$

III. ANALYTICAL CALCULATIONS

The analytical solution for the electrical domain of the anode (Eqs. (12) and (24)) were programmed within MATLAB (Mathworks, Natick, MA). This analytical solution can handle infinitely large model dimensions while maintaining a high accuracy. However, it includes some assumptions. These assumptions were: (1) within the PEDOT the current flow was only assumed perpendicular to the grid lines, (2) the effects of the bus bar were not taken into account (location of the anode connection), (3) the bus bar and cathode resistance was not taken into account, and (4) the j-V is linearized at a certain brightness. Assumptions 1 and 2 are correct when the length of the gridline (dimension of the OLED) is much larger than the grid pitch. In most cases, this will be easily obtained, as producers of OLEDs will aim at minimal visibility of the grids. Hence, grid widths will be minimized and a smaller grid width will also require a smaller grid pitch to still obtain acceptable light homogeneities. Assumption 4 results in a conductivity of the LEP layer which is dependent on the voltage/electric field. Due to the linearization of the j-V curve, this dependence is reasonable correct when the light output distribution of the OLED device is close to the linearization point. However, the conductivity is also known to be dependent on the carrier concentration and temperature.[11–13] The analytical model does not take this into account. In case of an inhomogeneous temperature distribution, caused by joule heating, the analytical model will not provide a correct solution.

To determine the effect of these assumptions, the homogeneity of the light emission of large area devices was also calculated numerically using FEM.[7] FEM allows modeling of very complex grid geometries without the analytical simplifications or assumptions, but often a limited computer memory (and time) places a practicality restriction on the dimensions of the model. The FEM model was used as a benchmark and as a check for the validity of the analytical assumptions.

The OLED design parameters in the model were defined as follows (see also Table I). The applied voltage was chosen such that a maximum light output of 5000 cd/m^2 for general lighting purposes was obtained. The grid, bus bar and cathode were assumed to be made of Aluminum, with an electrical conductivity which was 43% of the bulk conductivity (measured).

For the analytical model, the following dimensions were used (Figure 2): l = 1 mm, b1 = 0.1 mm, and l2 = 6 cm (Figure 6(a), note the difference in x and y dimensions). Symmetry is assumed along 3 boundaries (lower, right and upper boundary). In this way, one can model an OLED with a length of 12 cm and an "infinite width." Hence, it should be noted that the analytical model only models a unitcell area (e.g., Figure 2). The maximum and minimum light

TABLE I. Model properties.

	Width (m)	Thickness (m)	σ (S/m)
PEDOT		100×10^{-9}	4.0×10^{4}
LEP		80×10^{-9}	Linearized j-V Vth = 4.4 V, r = 0.012 m^2/AV
Grid	1×10^{-4}	440×10^{-9}	1.53×10^{7}
Bus bar	10×10^{-3}	440×10^{-9}	1.53×10^{7}
Cathode		100×10^{-9}	1.53×10^{7}

output within the unitcell are also the maximum and minimum light output for the cell.

Five comparisons between the analytical and numerical solutions were made:

1. using exactly the same assumptions for the numerical model as were made for the analytical model;
2. assuming a bus bar, the anode connection is along the complete length of the bus bar;
3. modeling a quarter of an OLED with a reduced element density (10 times less for the same volume);
4. including an anode connection on the bus bar;
5. including a cathode.

The FEM models, used for the first and second comparison, had the same dimensions as the analytical model; the dimensions of the unitcell (Figures 6(b) and 6(c)). The FEM models, used for the comparisons 3 to 5 were a quarter of a full 12×12 cm^2 OLED; hence 6×6 cm^2 (28 gridlines, Figures 6(d)–6(f)). COMSOL 3.5 a (Comsol AB, Stockholm, Sweden) was used to perform the FEM calculations. The light emitting polymer was modeled with solid volume elements, whereas the anode and cathode were modeled with a layer of 2D elements.

To verify the analytical model with the real working OLED, the light emission of a 12×12 cm^2 OLED was experimentally measured. The light-emitting polymer Lividux was used as emitter and the PEDOT:PSS anode consisted of Orgacon™ HILHC5. Material parameters and dimensions are given in Table I. The grid width and pitch were 0.2 mm and 2.2 mm, respectively.

The analytical approach was used to simulate the real working OLED. The dimensions of the model were 0.11 cm × 6.0 cm. The grid width is 0.1 mm. The dimensions of the unitcell are half the grid pitch (0.22 cm), half the grid width (0.2 mm), and half the experimental OLED dimension (12 cm). The unitcell is similar to the situation of Figure 2. The IVL was linearized around 500–600 cd/m^2, as that was the maximum light output of the experimental OLED. All other properties are given in Table I.

The analytical solution is applied to calculate the OLED grid design space for an OLED with the same PEDOT, LEP, and grid properties as discussed before (Table I). The grid

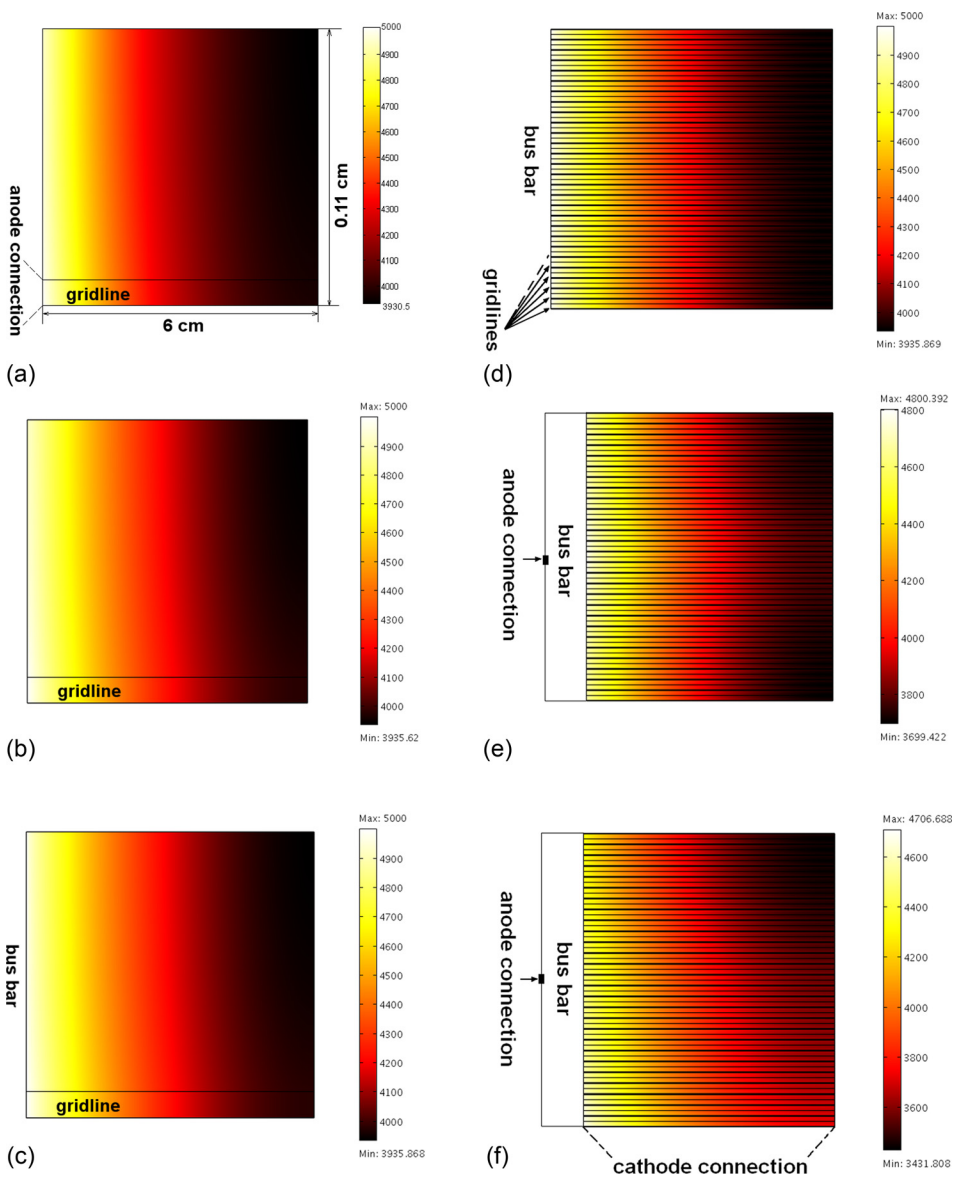

FIG. 6. (a) Brightness variation along the x and y coordinates of a 0.11 by 6 cm^2 OLED as obtained by our analytical model, ((b)–(f)) all obtained with COMSOL, (b) numerical simulation of the 0.11 by 6 cm^2 OLED, (c) show the effect of a bus bar, (d) a 6×6 cm^2 OLED with a reduced element density (quarter of 12×12 cm^2 OLED), (e) anode connection onto bus bar, and (f) cathode.

width and grid pitch were used as parametric input variables. The analytical equation was solved for the length of the OLED, assuming an allowed light drop of 20%.

IV. RESULTS AND DISCUSSION

Figure 6(a) shows the light distribution from a unitcell (like the situation in Figure 2) calculated with the analytical model. It is a topview of the unitcell where the light distribution below the gridline and the PEDOT:PSS is made visible. Note the difference in x and y dimension. Figure 6(b) shows the exact same situation but then simulated with FEM. The results are essentially undistinguishable. The minimum brightness at the top right of the OLED (Figure 6(a)) is 78.6% (−21.4%) of the brightness at the edge of 5000 cd/m^2 for both approaches (3931 cd/m^2 vs. 3936 cd/m^2). This light drop does not exactly match 20%. The reason for this is that for the current comparison, a grid design with just nice rounded dimensions was selected.

In these first two figures, the bus bar is omitted and the anode connection is just on the left edge of the grid line. Adding an actual aluminum bus bar (Figure 1), of which the complete left side is the anode connection (Figure 6(c)) leads to a negligible change (3936 cd/m^2) in comparison to analytical model (Figure 6(a)). If a quarter of the OLED is modeled within FEM with exactly the same boundary conditions as used for the simulation of Figure 6(c), the exact same minimum light output is achieved (Figure 6(d)). Note that in Figure 6(d) the x and y dimension are again scaled similarly. Although in this case, the element density, due to computer memory reasons, is much lower. This similar result indicates that a sufficient amount of elements was used in both simulations.

Adding a realistic anode contact on the bus bar (Figures 1 and 6(e)) leads to a small increase in light drop (from −21.4% to −22.9%, Figure 6(e)). And finally adding an Al based cathode with a thickness of 100 nm, instead of complete grounding of the bottom OLED area lead to a further increase in light drop to −27.1% (Figure 6(f)). However, note that the maximum light output is also reduced in the last two cases, from 5000 cd/m2 to 4800 and 4707 cd/m2, respectively.

Now having verified that the analytical model gives a very acceptable initial prediction for the light output of large area OLED devices, we compare the calculated light output distribution with experiments on a large-area OLED. To this purpose an OLED (12 by 12 cm^2) was fabricated on 15 by 15 cm^2 heat-stabilized Teonex® polyethylene naphtalate (PEN, DuPont Teijin Films) with a moisture barrier. The moisture barrier was stacked with a planarization layer to spatially separate defects in these films. PEDOT:PSS (Agfa Orgacon™ HILHC5, 100 nm) and the light-emitting polymer (Merck Livilux™, 80 nm) were deposited from solution by spin coating under ambient conditions. The cathode consisted of barium (5 nm)-aluminum (100 nm). The metallization around and within the active area was deposited by RF sputtering. The devices were encapsulated with the same thin film moisture barrier.

The measured homogeneity of the experimental OLED was roughly 84% at a brightness of 500–600 cd/m^2, comparing the value in the center of the OLED (Figure 7, distance: 6 cm) with the maximum value. This corresponded fairly well with the calculated homogeneity of the analytical model which was 81%, where the maximum and minimum light output was calculated to be 599.6 and 486.7 cd/m^2 at 5.35 V. Only the area near the bus bar (Figure 7, distance: 0–1 cm) showed a clearly different pattern in light output.

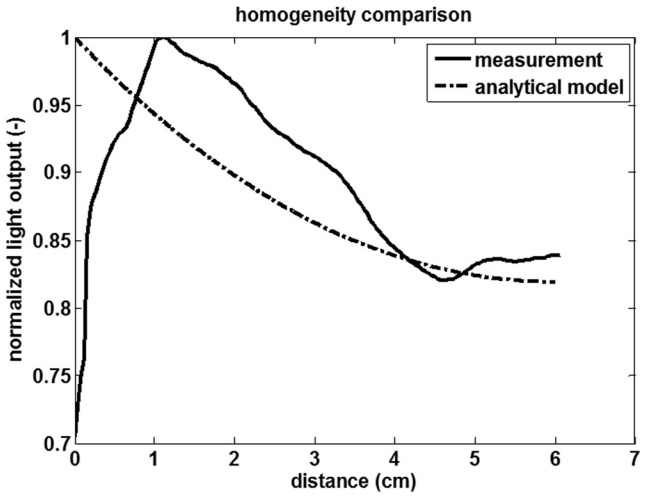

FIG. 7. Homogeneity comparison of experimental OLED and the analytical model.

An example of the OLED grid design space (for a 20% light drop) is given in Figure 8. The x and y axis display the grid width and grid pitch, according to Figure 1. The three different curves within the plot display different OLED dimensions (6 × 6 cm^2, 9 × 9 cm^2, and 12 × 12 cm^2). The combination of grid width and grid pitch of a certain curve, displays the combination of the grid and OLED dimensions which will result in a 20% light drop within the OLED. For example, if one would like to use 100 μm gridlines (grid width 0.1 mm), one can make a 12 × 12 cm^2 OLED using a grid pitch of ∼0.1 cm, a 9 × 9 cm^2 OLED using a grid pitch of ∼0.19 cm, and a 6 × 6 cm^2 OLED using a grid pitch of 0.36 cm. If one would like to manufacture an OLED with

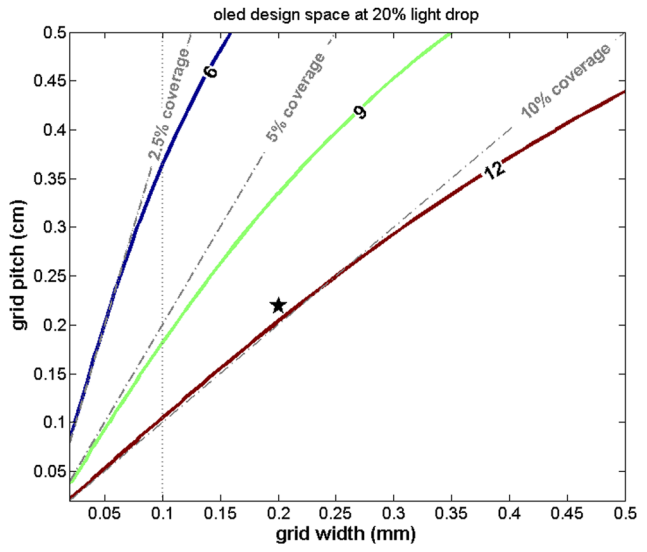

FIG. 8. Example plot of OLED design space at 20% light drop. The black star shows the settings of Figure 6(a).

only 2.5% grid coverage (and 20% light drop), then the figure shows that this limits the maximum size of the OLED to 6×6 cm^2. A possible option would be to use a grid width of approx. 0.0625 mm in combination width a grid pitch of 0.25 mm. Note also that fine grids (smaller grid widths and pitches) allow for larger OLEDs.

Increasing the grid width, when the grid width is still small, also allows for higher grid pitches. Hence, in that case, the limiting factor is the grid width; the largest voltage drop will occur within the grid. This is also clearly visible in Figure 6 where the voltage drop is along the gridline (note the corresponding star in Figure 8). Increasing already large grid widths leads to less increase in grid pitch (as the slope of all curves decreases) indicating that the grid pitch becomes the limiting factor. The largest voltage drop will then take place within the PEDOT.

V. CONCLUSION

In this paper, an analytical solution is presented for the light output of infinitely large sized OLEDs with parallel equidistant metal gridlines. The calculated light output of the model was verified with the measured light output of an experimental OLED and the assumptions within the model were verified with FEM calculations. The results clearly show that the voltage drop within the grid lines cannot be neglected. The voltage drop along the gridline becomes a more important issue with larger OLED sizes like the OLED size of 144 cm^2 which was used in this study.

We show that this analytical approach provides a quick overview of the parameter space and the relations between the parameters for designing a large-area OLED.

ACKNOWLEDGMENTS

The Holst Centre is an open innovation research center founded by TNO and IMEC that is developing roll-to-roll production techniques for foil-based organic electronics and wireless autonomous transducer solutions, in cooperation with industry and universities. This particular research has been funded by the Dutch Ministry of Economic Affairs, Philips Research, Agfa, Solvay and DuPont Teijin Films. We gratefully acknowledge Paul Blom for his input and assistance on preparing the manuscript. We kindly acknowledge Merck for the light emitting polymers. This work has further been supported by the NMP-2011.1.4-5/295368 IM^{3}OLED Project of the Framework 7 program of the EU.

[1]J. W. Park, D. C. Shin, and S. H. Park, "Large-area OLED lightings and their applications," Semicond. Sci. Technol. **26**, 034002 (2011).
[2]J. Park, H. Ham, and C. Park, "Heat transfer property of thin-film encapsulation for OLEDs," Org. Electron. **12**, 227–233 (2011).
[3]J. Shinar and R. Shinar, "An overview of oranic light-emitting diodes and their applications," in *Comprehensive Nanoscience Technology* (Academic Press, 2011), Vol. 1, pp. 73–107.
[4]Y. S. Tyan, "Organic light-emitting-diode lighting overview," SPIE J. Photon. Energy **1**, 1–15 (2011).
[5]H. Wu, L. Ying, W. Yang, and Y. Cao, "Progress and perspective of polymer white light-emitting devices and materials," Chem. Soc. Rev. **38**, 3391–3400 (2009).
[6]S. Choi, S. J. Kim, C. Fuentes-Hernandez, and B. Kippelen, "ITO-free large-area organic light-emitting diodes with an integrated metal grid," Opt. Express **19**, A793–803 (2011).
[7]S. Harkema, S. Mennema, M. Barink, H. Rooms, J. S. Wilson, T. Van Mol, and D. Bollen, "Large area ITO-free flexible white OLEDs with Orgacon PEDOT:PSS and printed metal shunting lines," Proc. SPIE **7415**, 74150T (2009).
[8]K. Neyts, A. Real, M. Marescaux, S. Mladenovski, and J. Beeckman, "Conductor grid optimization for luminance loss reduction in organic light emitting diodes," J. Appl. Phys. **103**, 093113/1–5 (2008).
[9]J. Park, J. Lee, D. Shin, and S. Park, "Luminance uniformity of large-area OLEDs with an auxiliary metal electrode," IEEE/OSA J. Disp. Technol. **5**(8), 306–311(2009).
[10]L. Pohl, E. Kollár, A. Poppe, and Z. Kohári, "Nonlinear electro-thermal modeling and field-simulation of OLEDs for lighting applications I: Algorithmic fundamentals," Microelectron. J. **43**(9), 624–632 (2012).
[11]W. F. Pasveer, J. Cottaar, C. Tanase, R. Coehoorn, P. A. Bobbert, P. W. M. Blom, D. M. De Leeuw, and M. A. J. Michels, "Unified description of charge-carrier mobilities in disordered semiconducting polymers," Phys. Rev. Lett. **94**, 20 (2005).
[12]L. Wang, H. Zhang, X. Tang, C. Mu, and J. Li, "An improved unified description of charge-carrier mobilities in disordered organic semiconductors," Curr. Appl. Phys. **10**, 1182–1187 (2010).
[13]L. Jun, S. Jiu-Xun, and C. Zhao, "Improved expression of charge-carrier mobility in disordered semiconducting polymers considering dependence on temperature, electric field and charge-carrier density," Synth. Met. **159**, 1915–1921 (2009).